Millimeter-Wave Beam-Steering Antenna Using a Fluidically Reconfigurable Lens

Ian Goode and Carlos E. Saavedra

***Abstract*— A fluidically reconfigurable millimeter-wave (mm-wave)-lensed antenna is reported that covers the band from 32 to 35 GHz. The antenna is a modified antipodal Vivaldi antenna element with a fluidically loaded dielectric lens to facilitate single-element beam-steering. The fluid used in this work is ethyl acetate ($C_4H_8O_2$) with $\epsilon_r = 5.0 + j1.3$, $\tan\delta = 0.26$ at 33.5 GHz. The antenna element and lens are manufactured using a substrate with $\epsilon_r = 3.55$ and $\tan\delta = 0.0027$. Experimental results show that the antenna can produce up to 25° of beam-steering at 32 GHz and up to 20° of beam-steering at 35 GHz. The maximum realized gain of the antenna is 8.6 dBi and the minimum realized gain is 5.6 dBi over the band.**

***Index Terms*— Antennas, antipodal Vivaldi, beam-steering, dielectric fluid, ethyl acetate, fluidic, lens, lensed antenna, microfluidics, microwave, millimeter-wave (mm-wave), planar antenna.**

I. Introduction

RECONFIGURABLE-LENSED antenna elements are attractive as they allow for adaptable radiation patterns, primarily beam-steering from a single element. In recent publications, single element beam-steering has been reported with a rotatable Luneburg-like lens [1], a mechanically movable lens [2], and by moving elements over a lens [3]. The referenced works operate by re-distributing dielectric material above the antenna aperture; however, they rely on mechanical actuation systems to steer the beam. Beam-steering has been seen with Luneburg lenses by moving the feed point around the perimeter of the lens by switching multiple elements around a lens [4] or by mechanically moving an antenna around a Luneburg lens [3], [5].

Microwave or mm-wave lenses are often made from a uniform dielectric material that is shaped to obtain the desired beam-forming characteristics [6]. Other types of lenses like a Luneburg lens or a Maxwell Fisheye lens have a variable relative permittivity across their radius to give beam-forming and beam-steering [7]. Lensed antennas have been used with wideband antennas [8], [9]. In [8], a simple dielectric lens is added to an antipodal Vivaldi element to improve the radiation pattern. In [9] a Luneburg lens was made using metamaterials for pattern improvements of a Vivaldi antenna. Further, variably permittivity lenses can be made using a substrate perforated with a periodic pattern of holes to improve the impedance bandwidth and gain of the antenna [10].

Millimeter-wave beam-steering has been seen by rotating a dual-sided polyethylene lens over a horn antenna to realize beam steering from a single element [2]. More advanced lensing techniques use a Luneburg lens where the antenna is scanned around the perimeter of the lens mechanically [3], [5], [11] or multiple antennas are electrically switched [4], [12] for beam-steering.

In many beam-steering lenses, physical movement of the lens is needed to observe the desired effect [1]–[3], [5], [11]; however, this mechanical actuation can be avoided using a dielectric fluid to change the properties of the lens to obtain beam-steering. Lenses with fluidic actuation have an extended lifetime when compared with other actuation methods, as the fluid can be hermetically sealed and moved about using electrowetting. While fluidic tuning of antennas and RF components is well established [13]–[23], no works have yet explored in detail the design of fluidically reconfigurable microwave or mm-wave lenses and only [24] has reported a fluidic lens with a variable focus at optical frequencies.

This article reports a millimeter-wave antenna with a fluidically reconfigurable cylindrical dielectric lens that can be reconfigured by filling holes in the lens with ethyl acetate. This lens can be reconfigured for single-element beam-steering covering the range 32–35 GHz. The antenna element is an antipodal Vivaldi and the lens is made by drilling holes into the antenna substrate. To increase the volume of fluid, the lens region of the antenna is made thicker by stacking two layers of substrate. While the fluidically reconfigurable lensed antenna discussed in this work was fabricated on a rigid substrate, it can be entirely implemented on a low-loss polymer compound, such as polydimethylsiloxane (PDMS). PDMS substrates are frequently used in wearable flexible electronics. The field of wearable flexible antennas has grown substantially in recent years. Examples include ink-jet printed antennas [25], Vivaldi antennas with flexible substrates for pattern improvement [26], and fluidically tuned antennas using liquid metals in flexible substrates for frequency tunable antennas [14], [27]. To the best of the authors' knowledge, this is the first use of fluidically reconfigurable mm-wave lensed antenna for beam-steering reported in the literature.

Manuscript received October 28, 2019; revised June 11, 2020; accepted July 3, 2020. Date of publication August 19, 2020; date of current version February 3, 2021. This work was supported in part by the Natural Sciences and Engineering Research Council of Canada (NSERC) under Grant #RGPIN-2016-04784. *(Corresponding author: Ian Goode.)*

The authors are with the Department of Electrical and Computer Engineering, Queen's University, Kingston, ON K7L 3N6, Canada (e-mail: ian.goode@queensu.ca; saavedra@queensu.ca).

Color versions of one or more of the figures in this article are available online at https://ieeexplore.ieee.org.

Digital Object Identifier 10.1109/TAP.2020.3016429

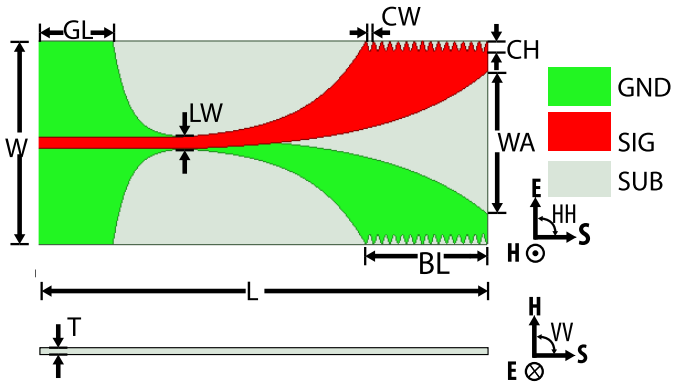

var.	L	W	LW	WA	BL	GL	CW	CH	T
(mm)	45	20	1.2	12	12	8	0.8	1	1.5

Fig. 1. Antipodal Vivaldi element with corrugations designed on 0.5 mm Rogers R04003C substrate prior to the addition of the lens. The two axes show the two orientations of the primary radiation pattern sweeps.

II. Antenna Element and Lens Design

The base element used here is a antipodal Vivaldi antenna with corrugated edges depicted in Fig. 1. This section details the design and integration of the fluidically reconfigurable dielectric lens onto the Vivaldi antenna element. This design started with full wave electromagnetic simulations in ANSYS HFSS.

The conventional approach for beam-steering using a Luneburg lens is to physically move the source around the perimeter of the lens [3], [5], [11]. Instead of mechanical actuation, multiple antennas located around the lens can be switched to move the source [4], [12] or a rotatable Luneburg lens with a modified distribution of dielectric material can be used for beam-steering [1]. The lens proposed in this work uses a dielectric fluid to load a cylindrical dielectric lens asymmetrically to facilitate beam-steering. In the fluidically loaded dielectric lens, a region of the hole-perforated lens is filled with dielectric fluid to steer the beam in that direction. To change the beam's direction, the fluid is moved to a different region of the lens. The lens was designed in a two-part process. First the beam-steering was simulated by moving an offset cylinder of dielectric around a cylindrical lens. The model was updated by adding a dielectric lens with holes that can be filled with fluid to facilitate beam-steering to emulate the shape of the offset lens.

Lens Geometry: The lens design started by adding a solid cylindrical dielectric lens to the end of the Vivaldi element, shown as the leftmost circle in Fig. 2(a). The dimensions and location of the cylindrical lens were varied to focus and sharpen the radiated beam across the operating band. Next, a second cylindrical dielectric lens was added with an offset to the first as shown in Fig. 2(b). Beam-steering was seen in simulation by rotating this offset cylinder. The offset cylinder added dielectric material on one side of the element to asymmetrically slow the propagation velocity through that region, causing the beam to steer. The offset distance between the cylindrical lenses was varied in simulation to find an optimal combination of beam-steering and peak-gain.

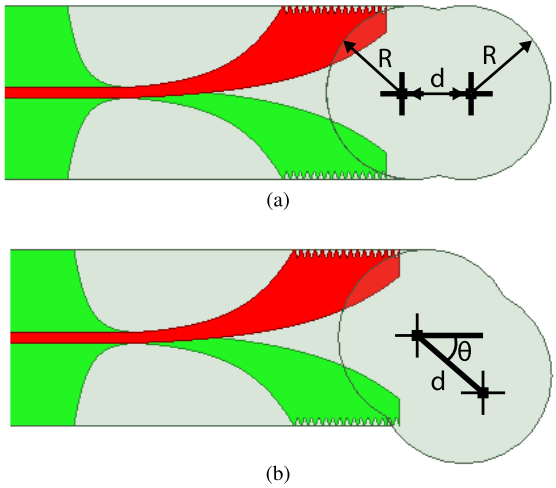

var.	d	R	θ
(mm)	5	10	-45°

Fig. 2. Antenna element with offset cylindrical lens at (a) 0° and (b) 45°. This offset angle is varied in simulation to provide beam-steering.

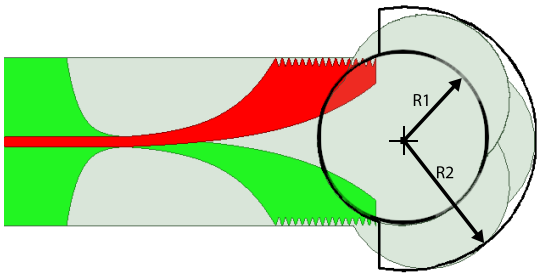

var.	$R1$	$R2$
(mm)	10	16

Fig. 3. Outline of the final lens is overlaid in black on the offset lens, which is rotated at three angles of $\theta = 0°, \pm 60°$. The inner region, $R1$ is always filled with substrate, whereas the outer region includes dielectric material based on θ. This outer region shows the area of the final lens that will be perforated with holes that can be filled with dielectric fluid.

Next, the lens was modified so that the distribution of dielectric material could be moved using fluids, rather than rotating the lens in simulation. When the offset lens is swept over the range $-60° \leq \theta \leq 60°$, the result traces out the structure in Fig. 3. The inner circle (R1) is the region that is always filled with dielectric material. The outer region $R1 \leq R \leq R2$ is sometimes filled with dielectric material depending on the offset angle θ. This outer region of the lens will be perforated so that it can be variably filled with fluid.

Fluidic Lens Design: The holes which hold the dielectric fluid to control the beam-steering are drilled around the outer perimeter of the lens as shown in Fig. 4. These holes line up with the region between $R1$ and $R2$ in Fig. 3 to emulate the action of rotating the offset lens in Fig. 2. The empty holes represent the area without substrate in Fig. 2. When the holes are filled with ethyl acetate, they locally increase the effective permittivity of the lens. The final structure shown in Fig. 4 is a lens that has a two-step dielectric permittivity profile.

Ethyl acetate ($\epsilon_r = 5.0 + j1.3$, $\tan\delta = 0.26$ at 33.5 GHz measured using the Keysight N1501A Material Measurement Performance Probe Kit) was chosen as the working dielectric

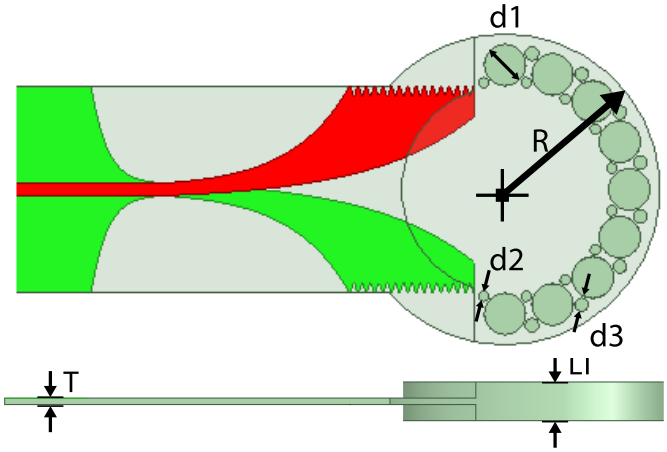

var.	R	$d1$	$d2$	$d3$	T	LT
(mm)	16	4	1	1.3	0.5	3.5

Fig. 4. Model of the designed fluidic lens with holes that can be filled with fluid. The fluid holes are located between $R1$ and $R2$ from Fig. 3 and are dimensioned to maximally fill this area.

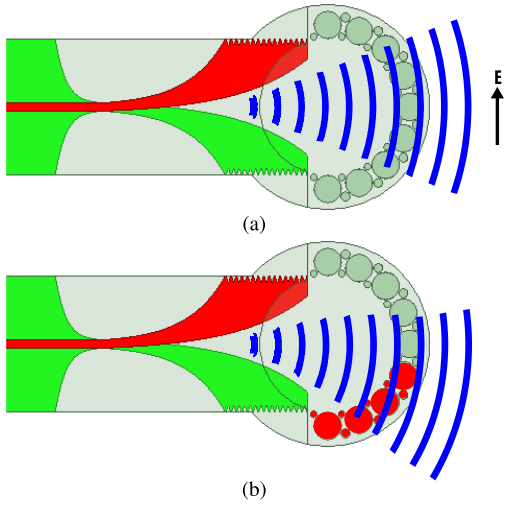

Fig. 5. Beam-steering on loaded lens, the shaded holes in the lens represent holes that are loaded with ethyl acetate (b) and in (a) all holes are air filled and no beam-steering is seen. Here the blue lines represent a wavefront to show beam-steering.

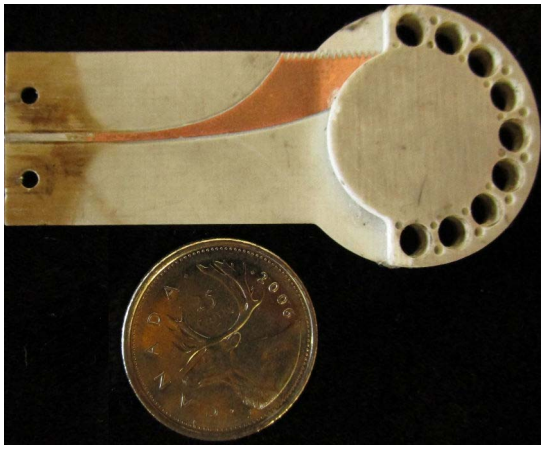

Fig. 6. Image of fabricated lensed element.

fluid as its relative permittivity is greater than the relative permittivity of the lens, but is low enough to avoid a large discontinuity in the impedance of the media when the lens is loaded with either fluid or air. Additionally, ethyl acetate was chosen as it has a lower loss tangent relative to other dielectric fluids with relative permittivity between 5 and 10.

The holes in Fig. 4 are selectively filled to emulate the shape of the offset lens at different angles of θ to see beam-steering. Large holes with a diameter $d_1 = 4$ mm were perforated around the perimeter of the lens. Two additional rows of holes of smaller size, $d_2 = 1$ mm and $d_3 = 1.3$ mm were added to increase the density of holes and provide greater versatility in the amount and location of fluid that could be added to the lens. Additional pieces of base antenna substrate (Rogers 4003C) were cut and stacked above and below the substrate of the antenna as depicted in the cross section drawing in Fig. 4. Identical holes were drilled in all three layers of the lens to increase the volume of ethyl acetate in each hole.

Fig. 5(a) graphically illustrates outgoing beam when all the holes in the lens are air-filled and Fig. 5(b) shows the beam-steering effect when a region of the lens is filled with ethyl acetate (red-colored holes). The beam is steered towards the ethyl acetate filled holes as was expected from the rotated offset lens in Fig. 2.

The antenna and lens structure were fabricated in-house using an LPKF Laser & Electronics AG milling machine. The substrate was 0.5 mm thick and the lens was 3.5 mm thick by layering additional pieces of 1.5 mm Rogers 4003C ($\epsilon_r = 3.55$ and $\tan\delta = 0.0027$) substrate above and below the substrate of the element. The thick part of the lens was made by stacking and adhering pieces of substrate to each other using pieces of thin, double-sided PDMS tape, ARseal 90880. To stop the fluid from draining out of the bottom, tape was applied to the ground plane side of the lens. The tape was not modeled in simulation due to a lack of permittivity and loss tangent data for the material. However, the lensed element was measured with and without the bottom tape for the air-filled case and no appreciable difference in peak gain or pattern shape across the band was observed.

III. Measured Results

Radiation pattern measurements were taken at Queen's University's anechoic chamber and all measured data is presented as realized gain. The system uses a signal generator (Anritsu—MG3694A) to produce a single tone that is then amplified and transmitted through a standard gain horn and the antenna under test (AUT) is rotated through the illuminated area in the $\vec{E}$- and $\vec{H}$-plane cuts. The AUT is then connected to a 50 Ω coaxial cable and connected to a microwave power meter (Anritsu—ML2437A). The system then gives realized gain by calculating the system losses and path-losses using a standard gain horn where the standard gain is provided as realized gain. In this setup, the gain loss from the impedance mismatches between the test antenna and the 50 Ω measurement setup is included. Input reflection data were measured using an Anritsu MS4644B vector network analyzer calibrated using an Anritsu 3652A-2 coaxial calibration kit.

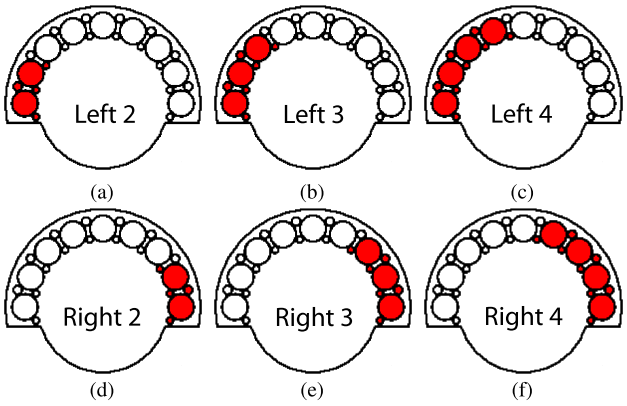

Fig. 7. Six filling combinations used with ethyl acetate for the high frequency lensed Vivaldi. The same nomenclature is used for all legends in this section. These figures show the lens in the same orientation as Fig. 6(a). The red filled holes show the holes that are filled with ethyl acetate, and the nonfilled holes are air-filled for each setup. (a) Left 2. (b) Left 3. (c) Left 4. (d) Right 2. (e) Right 3. (f) Right 4.

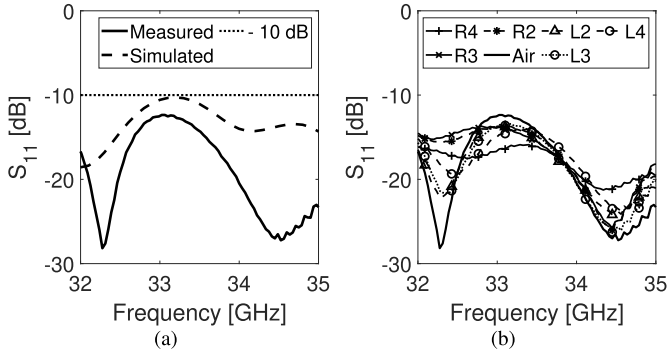

Fig. 8. (a) Measured input reflection for the high frequency lensed Vivaldi with all holes air-filled. (b) Measured input reflection for all filling cases for the high frequency fluidic lens.

TABLE I
SUMMARY OF BEAM-STEERING AT 33.5 GHz

Filling	Peak Gain (dBi)	Steer Angle (deg)	HPBW* (deg)
Left 4	7.4	-12	13
Left 3	7.3	-10	16
Left 2	7.3	-8	18
Air	8.2	0	15
Right 2	7.5	6	20
Right 3	7.2	12	21
Right 4	6.4	14	12

* Half Power Beam Width

The six liquid-filling patterns shown in Fig. 7 were used to test the behavior of the lensed antenna. The baseline case where all the holes are air-filled was also characterized. The six liquid-filled combinations were chosen from the simulated data to provide beam-steering while minimizing the impact on the peak realized gain.

The measured input reflection coefficients of the antenna element for the air-filled case and for the six filling patterns are shown in Fig. 8(a) and (b), respectively. For the measured input reflection as seen in Fig. 8(b) the addition of the ethyl acetate has a minor impact on the element's impedance match and its −10 dB impedance bandwidth remains unchanged for all filling combinations.

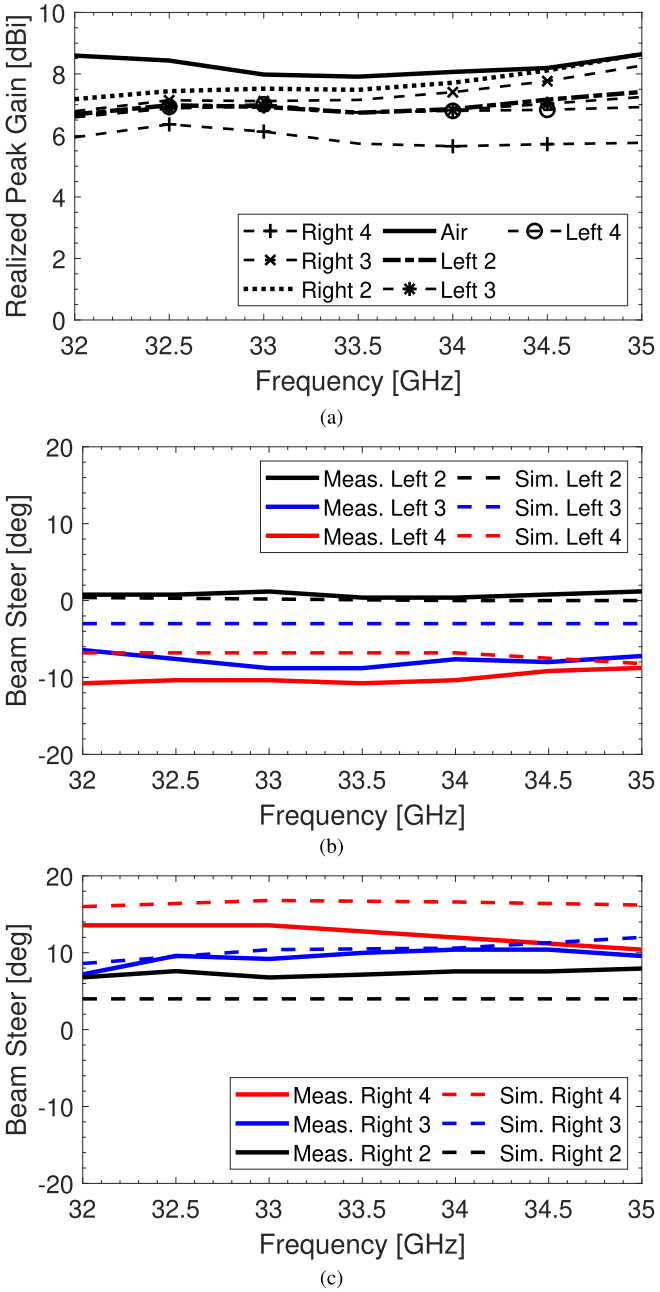

Fig. 9. (a) Measured peak realized gain for all fillings across the operating band of the element under all used filling conditions for the fluidic lens. (b) and (c) Measured and simulated beam-steering across the three left (b) and three right (c) used states for the high frequency fluidic lens.

The measured peak realized gain of the antenna for the seven filling conditions is plotted in Fig. 9(a). Here the peak gain was taken from the $\vec{E}$-plane measurement when the test antenna's steered beam was pointing at the transmitter with all fluidic holes being air-filled. The highest measured realized gain is 8.3±0.4 dBi for the air-filled case over the 32–35 GHz band and the minimum realized gain is 5.9±0.5 dBi for the right 4 case. The decrease in peak realized gain with an increase in the number of filled holes is due to the loss tangent of the ethyl acetate.

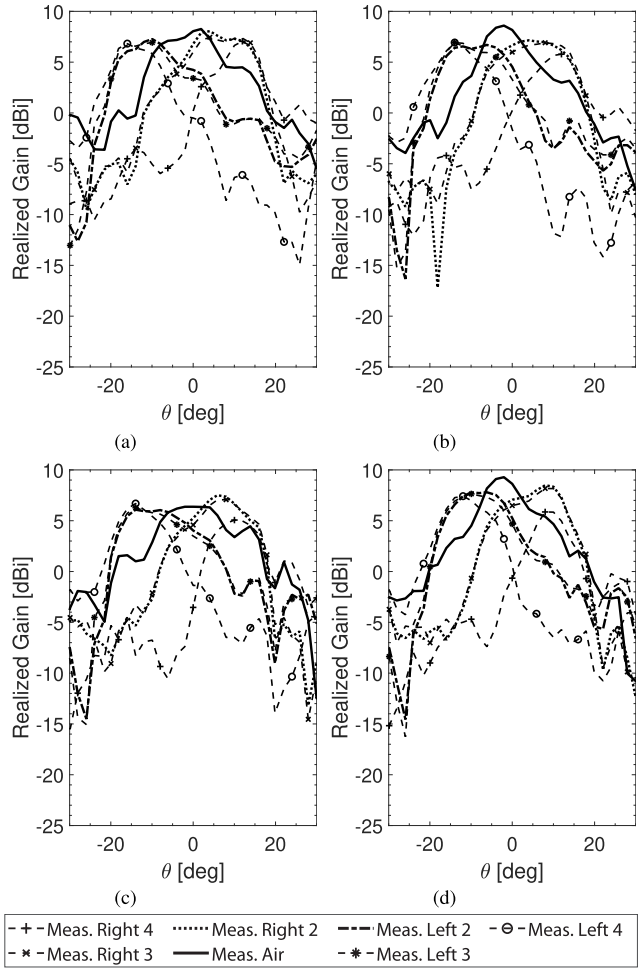

Fig. 10. Measured radiation pattern in the $\vec{E}$-plane for the seven beam filling states with each pattern show measured realized gain. The θ sweep is limited to the range $-30° \leq \theta \leq 30°$ to emphasize the beam-steering. (a) 32 GHz, (b) 33 GHz, (c) 34 GHz, and (d) 35 GHz.

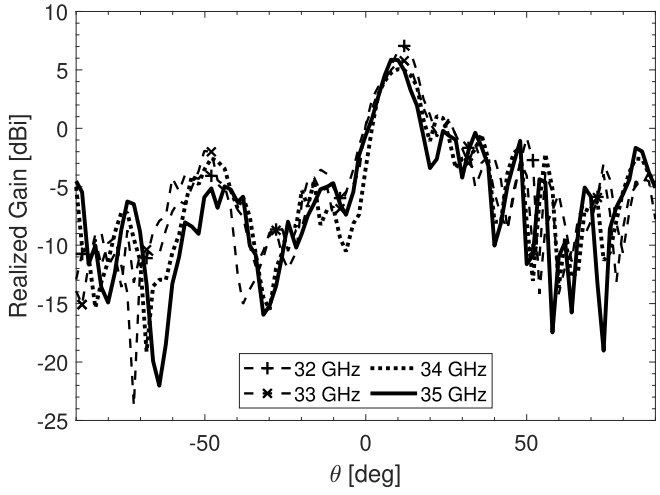

Fig. 11. Measured radiation patterns for $-90° \leq \theta \leq 90°$ for all the frequencies presented in Fig. 10. Showing the Right 4 filling.

The measured and simulated broadband beam-steering is compared in Fig. 9(b) and (c). The measured results show that the lensed antenna can produce up to 25° of beam-steering at 32 GHz and up to 20° of steering at 35 GHz. Table I summarizes the beam-steering performance at 33.5 GHz.

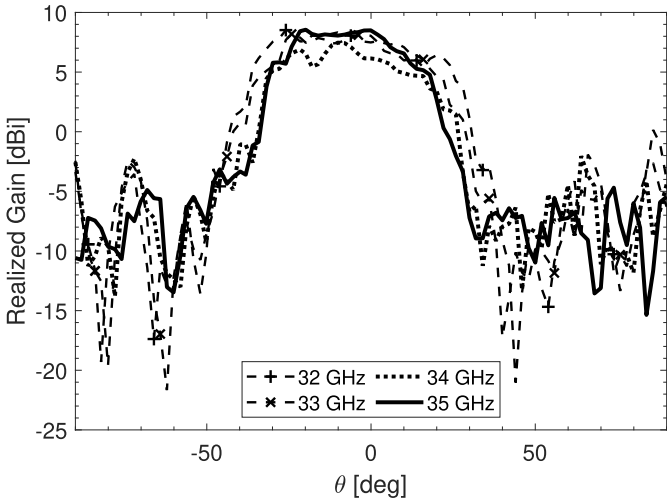

Fig. 12. Measured radiation pattern in the $\vec{H}$-plane or all of the frequencies presented in Fig. 10 for the air-filled case.

Fig. 10 shows the antenna's realized gain radiation patterns for the seven beam-steering states at four different frequencies. The data is plotted over the range $-30° \leq \theta \leq 30°$. A wide-angle sweep of the antenna radiation pattern over the range $-90° \leq \theta \leq 90°$ is shown in Fig. 11 for the case of maximum beam steer from 32–35 GHz. The wide-angle scan shows that the side-lobes are more than 8 dB below the main beam.

The antenna's measured realized gain radiation pattern in the $\vec{H}$-plane for the air-filled case is plotted in Fig. 12 from 32–35 GHz.

IV. Conclusion

Through this work, the design and measurement of a single element fluidically steerable lensed antenna was seen. This antenna covered a band of 32–35 GHz and was able to realize up to 25° of beam-steering with seven incremental beam-steering states. This work showed usable fluidically reconfigurable beam-steering from a single antenna element, which is the first known application of a fluidically loaded lens at mm-wave frequencies.

Acknowledgment

Ian Goode was a recipient of the Ontario Graduate Scholarship from the Province of Ontario, Canada, and the Ian M. Drum Scholarship from Queen's University.

References

[1] B. Zhou, Y. Yang, H. Li, and T. J. Cui, "Beam-steering vivaldi antenna based on partial luneburg lens constructed with composite materials," *J. Appl. Phys.*, vol. 110, no. 8, Oct. 2011, Art. no. 084908.

[2] J. R. Costa, E. B. Lima, and C. A. Fernandes, "Compact beam-steerable lens antenna for 60-GHz wireless communications," *IEEE Trans. Antennas Propag.*, vol. 57, no. 10, pp. 2926–2933, Oct. 2009.

[3] N. Nikolic and A. Hellicar, "Fractional luneburg lens antenna," *IEEE Antennas Propag. Mag.*, vol. 56, no. 5, pp. 116–130, Oct. 2014.

[4] Y. Song Zhang and W. Hong, "A millimeter-wave gain enhanced multi-beam antenna based on a coplanar cylindrical dielectric lens," *IEEE Trans. Antennas Propag.*, vol. 60, no. 7, pp. 3485–3488, Jul. 2012.

[5] A. R. Weily and N. Nikolic, "Dual-polarized planar feed for low-profile hemispherical Luneburg lens antennas," *IEEE Trans. Antennas Propag.*, vol. 60, no. 1, pp. 402–407, Jan. 2012.

[6] S. Silver, *Microwave Antenna Theory and Design*. no. 19. London, U.K.: IET, 1984.
[7] Y. T. Lo and S. Lee, *Antenna Handbook: Theory, Applications, and Design*. New York, NY, USA: Springer, 2013.
[8] M. Amiri, F. Tofigh, A. Ghafoorzadeh-Yazdi, and M. Abolhasan, "Exponential antipodal vivaldi antenna with exponential dielectric lens," *IEEE Antennas Wireless Propag. Lett.*, vol. 16, pp. 1792–1795, 2017.
[9] A. Dhouibi, S. N. Burokur, A. de Lustrac, and A. Priou, "Compact metamaterial-based substrate-integrated luneburg lens antenna," *IEEE Antennas Wireless Propag. Lett.*, vol. 11, pp. 1504–1507, 2012.
[10] M. Asaadi and A. Sebak, "Gain and bandwidth enhancement of 2×2 square dense dielectric patch antenna array using a holey superstrate," *IEEE Antennas Wireless Propag. Lett.*, vol. 16, pp. 1808–1811, 2017.
[11] B. Fuchs, O. Lafond, S. Rondineau, M. Himdi, and L. L. Coq, "Off-axis performances of half maxwell fish-eye lens antennas at 77 GHz," *IEEE Trans. Antennas Propag.*, vol. 55, no. 2, pp. 479–482, Feb. 2007.
[12] Z. Briqech, A.-R. Sebak, and T. A. Denidni, "Wide-scan MSC-AFTSA array-fed grooved spherical lens antenna for millimeter-wave MIMO applications," *IEEE Trans. Antennas Propag.*, vol. 64, no. 7, pp. 2971–2980, Jul. 2016.
[13] J.-H. So, J. Thelen, A. Qusba, G. J. Hayes, G. Lazzi, and M. D. Dickey, "Reversibly deformable and mechanically tunable fluidic antennas," *Adv. Funct. Mater.*, vol. 19, no. 22, pp. 3632–3637, Nov. 2009.
[14] G. J. Hayes, J.-H. So, A. Qusba, M. D. Dickey, and G. Lazzi, "Flexible liquid metal alloy (EGaIn) microstrip patch antenna," *IEEE Trans. Antennas Propag.*, vol. 60, no. 5, pp. 2151–2156, May 2012.
[15] M. Konca and P. A. Warr, "A frequency-reconfigurable antenna architecture using dielectric fluids," *IEEE Trans. Antennas Propag.*, vol. 63, no. 12, pp. 5280–5286, Dec. 2015.
[16] C. Borda-Fortuny, K.-F. Tong, A. Al-Armaghany, and K.-K. Wong, "A low-cost fluid switch for frequency-reconfigurable vivaldi antenna," *IEEE Antennas Wireless Propag. Lett.*, vol. 16, pp. 3151–3154, 2017.
[17] A. Singh, I. Goode, and C. E. Saavedra, "A multistate frequency reconfigurable monopole antenna using fluidic channels," *IEEE Antennas Wireless Propag. Lett.*, vol. 18, no. 5, pp. 856–860, May 2019.
[18] M. Brown and C. E. Saavedra, "Tunable branchline coupler using microfluidic channels," *IEEE Microw. Wireless Compon. Lett.*, vol. 29, no. 3, pp. 207–209, Mar. 2019.
[19] C. Murray and R. R. Franklin, "Independently tunable annular slot antenna resonant frequencies using fluids," *IEEE Antennas Wireless Propag. Lett.*, vol. 13, pp. 1449–1452, 2014.
[20] W. Su, B. Cook, M. Tentzeris, C. Mariotti, and L. Roselli, "A novel inkjet-printed microfluidic tunable coplanar patch antenna," in *Proc. IEEE Antennas Propag. Soc. Int. Symp. (APSURSI)*, Jul. 2014, pp. 858–859.
[21] D. Rodrigo, L. Jofre, and B. A. Cetiner, "Circular beam-steering reconfigurable antenna with liquid metal parasitics," *IEEE Trans. Antennas Propag.*, vol. 60, no. 4, pp. 1796–1802, Apr. 2012.
[22] G. B. Zhang, R. C. Gough, M. R. Moorefield, K. J. Cho, A. T. Ohta, and W. A. Shiroma, "A liquid-metal polarization-pattern-reconfigurable dipole antenna," *IEEE Antennas Wireless Propag. Lett.*, vol. 17, no. 1, pp. 50–53, Jan. 2018.
[23] I. Goode and C. E. Saavedra, "Ultra-wideband fluidically steered antipodal vivaldi antenna array," *Microw. Opt. Technol. Lett.*, vol. 62, no. 9, pp. 2938–2944, Sep. 2020.
[24] H. Choi and Y. H. Won, "Fluidic lens of floating water using intermediate hydrophilic layer based on electrowetting," *IEEE Photon. Technol. Lett.*, vol. 25, no. 18, pp. 1829–1831, Sep. 2013.
[25] B. K. Tehrani, B. S. Cook, and M. M. Tentzeris, "Inkjet printing of multilayer millimeter-wave yagi-uda antennas on flexible substrates," *IEEE Antennas Wireless Propag. Lett.*, vol. 15, pp. 143–146, 2016.
[26] L. Sang, S. Wu, G. Liu, J. Wang, and W. Huang, "High-gain UWB vivaldi antenna loaded with reconfigurable 3-D phase adjusting unit lens," *IEEE Antennas Wireless Propag. Lett.*, vol. 19, no. 2, pp. 322–326, Feb. 2020.
[27] K. Y. Alqurashi and J. R. Kelly, "Continuously tunable frequency reconfigurable liquid metal microstrip patch antenna," in *Proc. IEEE Int. Symp. Antennas Propag. USNC/URSI Nat. Radio Sci. Meeting*, Jul. 2017, pp. 909–910.

Ian Goode is originally from Peterborough, ON, Canada. He received the B.A.Sc. degree in engineering physics from Queen's University, Kingston, ON, in 2017, where he is currently pursuing the Ph.D. degree with the Department of Electrical Engineering.

He was the Chief Technical Officer of Rover Design for the Queen's Space Engineering Team (QSET) from 2016–2018, where he oversaw the full redesign of QSET's astronaut assistance vehicle prototype that competed in the University Rover Challenge. His current research interests include fluidically reconfigurable antennas and lensed antennas.

Mr. Goode has received multiple scholarships to support his graduate work, including the Ian M. Drum Scholarship in 2018 and the Ontario Graduate Scholarship in 2017 and 2020. He was a recipient of the 2019 IEEE Kingston Section M.A.Sc Research Excellence Award.

Carlos E. Saavedra received the B.Sc. degree from the University of Virginia, Charlottesville, VA, USA, and the M.Sc. and Ph.D. degrees from Cornell University, Ithaca, NY, USA, all in electrical engineering.

He is currently a Professor and the Head of the Department of Electrical and Computer Engineering, Queen's University, Kingston, ON, Canada. He is a registered Professional Engineer (P.Eng.) in the Province of Ontario. During sabbatical leaves, he has held visiting appointments at the University of Navarra, San Sebastían, Spain, the Universidade Federal of Rio Grande do Sul, Porto Alegre, Brazil, and the University of Twente, Enschede, The Netherlands. From 1998 to 2000, he was a Senior Engineer at Millitech Corporation, Northampton, MA, USA, where he was a Lead Designer for 38 GHz point-to-point broadband wireless transceivers.

Dr. Saavedra was a recipient of the NSERC Discovery Accelerator Award, he coauthored the Best Student Paper at the 2009 IEEE SiRF Conference, and he is a three-time recipient of the Undergraduate Teaching Award in Electrical Engineering at Queen's University. He co-chaired the Natural Sciences and Engineering Research Council of Canada (NSERC) Discovery Grant Evaluation Group for Electrical and Computer Engineering and he has served on grant review panels at the National Science Foundation (USA) and as an External Reviewer for the Netherlands Organisation for Scientific Research. He is a Guest Editor of the IEEE OPEN JOURNAL ON ANTENNAS AND PROPAGATION and is a former Associate Editor of the IEEE TRANSACTIONS ON MICROWAVE THEORY AND TECHNIQUES and a former Guest Editor of the *IEEE Microwave Magazine*.